

Light transfer transitions beyond higher-order exceptional points in parity-time and anti-parity-time symmetric waveguide arrays

Chuanxun Du¹, Gang Wang², Yan Zhang^{1,†}, and Jin-Hui Wu^{1,*}

¹ School of Physics and Center for Quantum Sciences,
Northeast Normal University, Changchun 130024, China

² School of Physical Science and Technology, Soochow University, Suzhou 215006, China

[†] zhangy345@nenu.edu.cn and

^{*} jhwu@nenu.edu.cn

We propose two non-Hermitian arrays consisting of $N = 2l + 1$ waveguides and exhibiting parity-time (\mathcal{PT}) or anti- \mathcal{PT} symmetry for investigating light transfer dynamics based on N th-order exceptional points (EPs). The \mathcal{PT} -symmetric array supports two N th-order EPs separating an unbroken and a broken phase with real and imaginary eigenvalues, respectively. Light transfer dynamics in this array exhibits radically different behaviors, *i.e.* a unidirectional oscillation behavior in the unbroken phase, an edge-towards localization behavior in the broken phase, and a center-towards localization behavior just at N th-order EPs. The anti- \mathcal{PT} -symmetric array supports also two N th-order EPs separating an unbroken and a broken phase, which refer however to imaginary and real eigenvalues, respectively. Accordingly, light transfer dynamics in this array exhibits a center-towards localization behavior in the unbroken phase and an origin-centered oscillation behavior in the broken phase. These nontrivial light transfer behaviors and their controlled transitions are not viable for otherwise split lower-order EPs and depend on the underlying $SU(2)$ symmetry of spin- l matrices.

PACS numbers:

I. INTRODUCTION

Hamiltonians in quantum mechanics are usually Hermitian and exhibit real eigenvalues, hence convenient for describing closed (conserved) systems with neither loss nor gain. Hermitian Hamiltonians in combination with perturbation methods may also be extended to describe open (non-conserved) systems involving loss or gain; nevertheless inevitably bring extensive calculations. By comparison, non-Hermitian Hamiltonians not only provide a straightforward framework for describing open systems [1–5], but also are explored to reveal quite a few unusual features unavailable for Hermitian Hamiltonians [6–10]. One prominent example is that two or more eigenvalues and eigenvectors of a non-Hermitian Hamiltonian can become degenerate under appropriate conditions, yielding the so-called exceptional points (EPs) [11–13]. So far realization and exploitation of EPs have been well investigated in various non-Hermitian systems especially those exhibiting, *e.g.* parity-time (\mathcal{PT}) symmetry [14–17] or anti-parity-time (anti- \mathcal{PT}) symmetry [18–20]. Typically, drastic changes of relevant phenomena would occur around EPs so that it is viable to realize switching of optical transmission [8, 21], topological phase transition [22–24], ultra-sensitive measurement [25–27], nonreciprocal light propagation [28–31], etc. These nontrivial findings are closely associated with the orders of EPs [32–36] because higher-order EPs usually involve more complicated physics and bring more interesting results [5, 37–41], though also more difficult to realize owing to higher requirements on the Hamiltonian symmetry [42–44].

Hinging on the mathematical isomorphism between the Schrödinger equation and the Maxwell paraxial wave

equation, investigations on non-Hermitian physics have been extended to and are flourishing in optics and photonics in view of the great convenience on experimental realizations [45–50]. Typical optical platforms for investigating non-Hermitian phenomena include arrays of resonators and waveguides described by engineered mode-coupling matrices with complex diagonal or off-diagonal elements [51–53]. It is found, for instance, light transport in two-mode \mathcal{PT} -symmetric waveguides with balanced gain and loss changes drastically from a reciprocal to a nonreciprocal behavior across the 2nd-order EPs of mode-coupling matrices [45, 46]. More interesting non-Hermitian characteristics and applications, such as richer topological photonics [54], enhanced spontaneous emission [55], improved sensitivity of spectra and dynamics [56–58], and delayed sudden death of entanglement [59], have also been found around higher-order EPs of mode-coupling matrices, *e.g.* in \mathcal{PT} -symmetric waveguide arrays discussed in terms of underlying $SU(2)$ symmetry [42]. Meanwhile, passive optical systems exhibiting anti- \mathcal{PT} symmetry have spurred a rapidly growing interest in that they hold unique non-Hermitian features [60–63] yet without the need of gain [64–66] limiting realistic implementations and applications. In this regard, multi-mode anti- \mathcal{PT} -symmetric waveguides deserve further studies on higher-order EPs and nontrivial light transport.

In this work we consider two non-Hermitian arrays consisting of $N = 2l + 1$ waveguides in the regimes of \mathcal{PT} symmetry and anti- \mathcal{PT} symmetry, respectively, for achieving two highest N th-order EPs and examining a few nontrivial light transfer behaviors. Mode-coupling matrices with imaginary diagonal (sub-diagonal) elements are constructed here for describing the \mathcal{PT} -

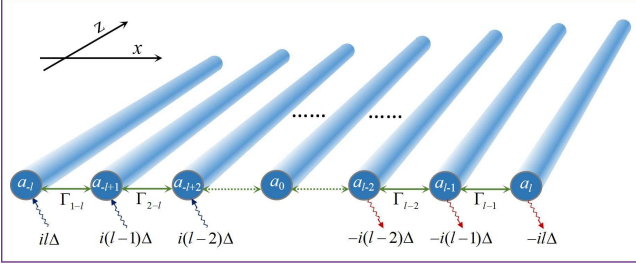


FIG. 1: A \mathcal{PT} -symmetric array of $2l + 1$ single-mode waveguides arranged (extending) along the x -axis (z axis). Each mode a_n exhibits an imaginary propagation constant $-in\Delta$ indicating balanced gain ($n < 0$) and loss ($n > 0$) for $\Delta > 0$ while two real coupling constants Γ_n and Γ_{n-1} (Γ_{n+1} and Γ_n) with its neighbors a_{n+1} and a_{n-1} , respectively, for $n > 0$ ($n < 0$).

symmetric (anti- \mathcal{PT} -symmetric) waveguide array on the basis of two spin- l matrices [43, 44] embodying the underlying $SU(2)$ symmetry. Different from the ballistic (breathing-like) light transport in a Hermitian waveguide array, the light transport in our \mathcal{PT} -symmetric waveguide array can be switched between a unidirectional oscillation behavior in the unbroken phase and an edge-towards localization behavior (related to the skin effect [67]) in the broken phase through a center-towards localization behavior at one N th-order EP. Such a sensitive transition of light transfer behaviors becomes impossible when both N th-order EPs are split into a series of lower-order EPs by modifying somehow the corresponding mode-coupling matrix. Compared to the

\mathcal{PT} -symmetric waveguide array with balanced gain and loss, the anti- \mathcal{PT} -symmetric waveguide array with passive couplings [65, 68–70] supports another transition between distinct light transfer behaviors around one N th-order EP: a center-towards localization behavior even in the unbroken phase and an origin-centered oscillation behavior in the broken phase.

II. \mathcal{PT} -SYMMETRIC WAVEGUIDE ARRAY

In this section, we start by considering in Fig. 1 an array consisting of $N = 2l + 1$ single-mode waveguides labeled by a_n for $n \in \{-l, l\}$. Our goal is to examine non-trivial light transfer behaviors based on N th-order EPs by constructing a \mathcal{PT} -symmetric mode-coupling matrix for this N -mode waveguide array with underlying $SU(2)$ symmetry. Generally speaking, N th-order EPs are viable to be observed via a fine tuning of propagation and coupling constants, though may be easily split into lower-order EPs even in case of a slightly broken N th-order $SU(2)$ symmetry. In principle, two N th-order EPs will be found at $\alpha = \pm\beta$ for an $N \times N$ non-Hermitian matrix $H_{non} = \alpha S_i + i\beta S_j$ ($i = x$ and $j = z$ or vice versa), being S_i (S_j) the Cartesian operator along the i -axis (j -axis) of a spin- l system [44]. Such non-Hermitian matrices have been adopted to describe various quantum or classical systems, including the Bose-Hubbard model [43], ultracold Bose gases [71], and waveguide arrays [58].

With above considerations, we construct the \mathcal{PT} -symmetric mode-coupling matrix

$$H = 2\Gamma S_x + i\Delta S_z = \begin{pmatrix} il\Delta & \Gamma_{1-l} & 0 & \cdots & 0 & 0 & 0 & 0 \\ \Gamma_{1-l} & -i(1-l)\Delta & \Gamma_{2-l} & \cdots & 0 & 0 & 0 & 0 \\ 0 & \Gamma_{2-l} & -i(2-l)\Delta & \ddots & \ddots & 0 & 0 & 0 \\ \vdots & \vdots & \ddots & \ddots & \ddots & \vdots & \vdots & \vdots \\ 0 & 0 & \ddots & \ddots & -i(l-2)\Delta & \Gamma_{l-2} & 0 & 0 \\ 0 & 0 & 0 & \cdots & \Gamma_{l-2} & -i(l-1)\Delta & \Gamma_{l-1} & 0 \\ 0 & 0 & 0 & \cdots & 0 & \Gamma_{l-1} & -il\Delta & 0 \end{pmatrix}, \quad (1)$$

with imaginary diagonal elements $H_{n,n} = -in\Delta$ for $n \in \{-l, l\}$ and real sub-diagonal elements $H_{n\pm 1,n} = H_{n,n\pm 1} = \Gamma_n$ restricted by $\Gamma_n = \Gamma\sqrt{(l \pm n + 1)(l \mp n)}$ for $n \in \pm\{0, l-1\}$. With respect to the waveguide array as illustrated in Fig. 1 [46], imaginary diagonal elements refer to gain or loss constants adjusted, *e.g.* by a temperature gradient [72, 73], while real sub-diagonal elements refer to adjacent couplings adjusted, *e.g.* by the

waveguide separations [74, 75]. To be more specific, the waveguide array described by Eq. (1) exhibits balanced gain and loss ($H_{-n,-n} = -H_{n,n} = in\Delta$) in the presence of a neutral ($H_{0,0} = 0$) central waveguide. On this basis, the mode-coupling matrix in Eq. (1) is found to be exactly \mathcal{PT} symmetric because it satisfies the commutation relation $[\mathcal{PT}, H] = 0$, where the parity operator \mathcal{P} indicates spatial reflection and is described by the standard

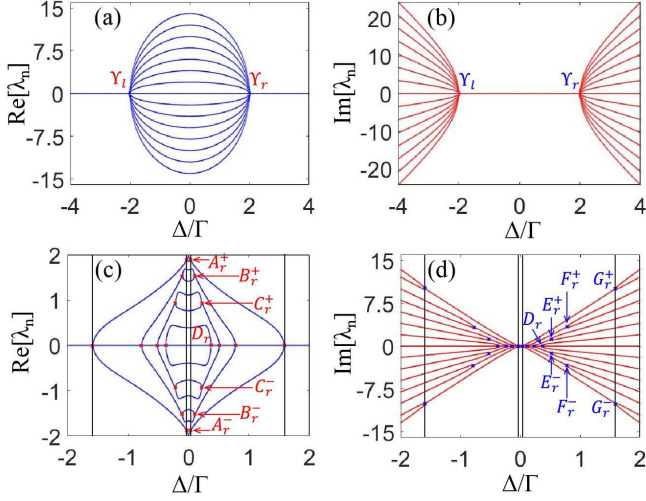


FIG. 2: (a) Real and (b) imaginary parts of $2l+1$ eigenvalues of \mathcal{PT} -symmetric mode-coupling matrix H in Eq. (1) against Δ/Γ with $\Gamma_n = \Gamma\sqrt{(l \pm n + 1)(l \mp n)}$ for $n \in \pm\{0, l-1\}$ and $l = 7$. (c) Real and (d) imaginary parts of $2l+1$ eigenvalues of \mathcal{PT} -symmetric mode-coupling matrix H in Eq. (1) against Δ/Γ with $\Gamma_n = \Gamma$ for $n \in \pm\{0, l-1\}$ and $l = 7$.

involutory permutation matrix

$$P = \begin{pmatrix} 0 & 0 & \cdots & 0 & 1 \\ 0 & 0 & \cdots & 1 & 0 \\ \vdots & \vdots & \ddots & \vdots & \vdots \\ 0 & 1 & \cdots & 0 & 0 \\ 1 & 0 & \cdots & 0 & 0 \end{pmatrix}, \quad (2)$$

while the time reversal operator \mathcal{T} indicates complex conjugation with $H^\dagger = \mathcal{T}H^T\mathcal{T} = \mathcal{T}H\mathcal{T}$.

We plot real parts in Fig. 2(a) while imaginary parts in Fig. 2(b) of eigenvalues λ_n of \mathcal{PT} -symmetric mode-coupling matrix H in Eq. (1) with $l = 7$. It is easy to see that all fifteen eigenvalues coalesce at $\Delta/\Gamma = \pm 2$ with $\lambda_n \equiv 0$, yielding thus two highest 15th-order EPs marked by Υ_l and Υ_r . It is more important that the \mathcal{PT} -symmetric waveguide array can be engineered on demand to work in the unbroken phase with purely real eigenvalues in the case of $|\Delta/\Gamma| < 2$, while in the broken phase with purely imaginary eigenvalues in the case of $|\Delta/\Gamma| > 2$. To clarify the importance of choosing proper sub-diagonal elements, we then make similar plots in Fig. 2(c) and Fig. 2(d) for another \mathcal{PT} -symmetric mode-coupling matrix where $\Gamma_n = \Gamma\sqrt{(l \pm n + 1)(l \mp n)}$ is replaced by $\Gamma_n = \Gamma$ for $n \in \pm\{0, l-1\}$. It is found that each 15th-order EP degrades into a dozen of 2nd-order EPs and a single 3rd-order EP. To be more specific, points Υ_l and Υ_r are split into groups $\{A_l^\pm, B_l^\pm, C_l^\pm, D_l, E_l^\pm, F_l^\pm, G_l^\pm\}$ (not shown) and $\{A_r^\pm, B_r^\pm, C_r^\pm, D_r, E_r^\pm, F_r^\pm, G_r^\pm\}$ (shown), respectively, in a way of exact mirror symmetry with respect to $\Delta/\Gamma = 0$. This then results in a very narrow unbroken phase between points A_l^\pm and A_r^\pm ; twelve partially broken phases

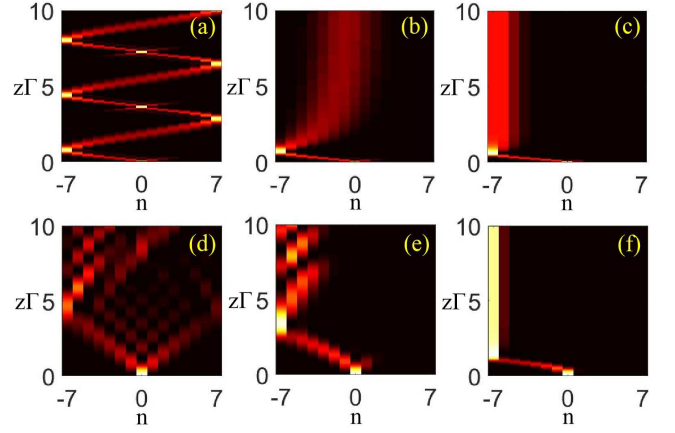


FIG. 3: Evolutions of mode excitations in a \mathcal{PT} -symmetric waveguide array with $\Gamma_n = \Gamma\sqrt{(l \pm n + 1)(l \mp n)}$ (a,b,c) or $\Gamma_n = \Gamma$ (d,e,f) for $n \in \pm\{0, l-1\}$ and $l = 7$ regarding the same initial excitation $a_n(0) = \delta_{n,0}$. The upper and lower panels are plotted with $\Delta/\Gamma = 1$ (a); $\Delta/\Gamma = 2$ (b); $\Delta/\Gamma = 4$ (c) and $\Delta/\Gamma = 0.02$ (d); $\Delta/\Gamma = 0.494$ (e); $\Delta/\Gamma = 3$ (f), respectively.

between points G_l^\pm and A_l^\pm as well as between points A_r^\pm and G_r^\pm ; two fully broken phases at the left of points G_l^\pm or at the right of points G_r^\pm .

As a light beam is incident upon one or more of the N waveguides, its longitudinal propagation along the z -axis and transverse transfer between adjacent waveguides evolve according to a Schrödinger-like equation $i\partial_z\psi = H\psi$ [45, 46]. Here an $N \times 1$ column vector $\psi = (a_{-l}, \dots, a_0, \dots, a_l)^T$ has been introduced to describe the collective excitation of this \mathcal{PT} -symmetric waveguide array, being a_n an excitation amplitude of the n th mode. Using the \mathcal{PT} -symmetric mode-coupling matrix H in Eq. (1), it is straightforward to expand the Schrödinger-like equation into

$$\frac{\partial a_n}{\partial z} = \begin{cases} -n\Delta a_n - i\Gamma_n a_{n-1} - i\Gamma_{n+1} a_{n+1} & (n < 0), \\ -i\Gamma_n (a_{n-1} + a_{n+1}) & (n = 0), \\ -n\Delta a_n - i\Gamma_{n-1} a_{n-1} - i\Gamma_n a_{n+1} & (n > 0), \end{cases} \quad (3)$$

restricted by the boundary conditions $n \in \{-l, l\}$ and $\Gamma_{-l-1} = \Gamma_{l+1} = 0$.

We examine with Eq. (3) evolutions of mode excitations characterized by $|a_n(z)|^2 / \sum_n |a_n(z)|^2$ in the \mathcal{PT} -symmetric waveguide array for a single-site initial excitation $a_n(0) = \delta_{n,0}$. Plotted with $\Delta/\Gamma = 1$ in the unbroken phase, Fig. 3(a) shows that the incident light first transfers unidirectionally toward waveguides of larger gain constants until reaching the left edge, then oscillates symmetrically between the left and right edges with a period $\delta z = 2\pi/\sqrt{4\Gamma^2 - \Delta^2}$. This is different from the (breathing-like) bidirectional Bloch oscillations observed in corresponding Hermitian waveguide arrays [72] because mode-coupling matrix H exhibits real eigenval-

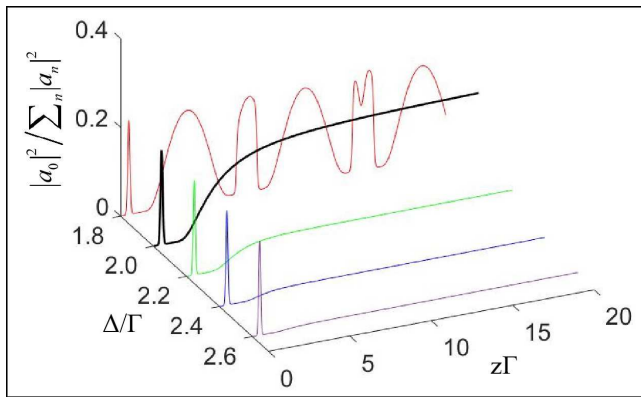


FIG. 4: Evolutions of central ($n = 0$) mode excitation referring to a few typical ratios of Δ/Γ in a \mathcal{PT} -symmetric waveguide array with $\Gamma_n = \Gamma\sqrt{(l \pm n + 1)(l \mp n)}$ for $n \in \pm\{0, l-1\}$ and $l = 7$ regarding the initial excitation $a_n(0) = \delta_{n,7}$.

ues and linearly gradient gain/loss constants. In other words, the unidirectional oscillation occurs only if an excitation transfer from the central ($n = 0$) waveguide is increasingly evanescent toward the right ($n > 0$) waveguides while increasingly amplified toward the left ($n < 0$) waveguides in an exactly asymmetric manner. Plotted with $\Delta/\Gamma = 2$ at one N th-order EP Υ_r , Fig. 3(b) shows that mode excitations are localized around the central waveguide with no oscillations after a single reflection from the left edge. This may be attributed to a strong centripetal force arising from the highest-degree degeneracy of all eigenvalues $\lambda_n \equiv 0$ and promises a robust directional output of mode excitations from the interface of middle waveguides with loss and gain respectively. Plotted with $\Delta/\Gamma = 4$ in the broken phase, Fig. 3(c) shows that mode excitations suffer neither oscillations nor reflections and are localized near the left edge instead, similar to the skin effect. This promises another robust directional output of mode excitations clinging to the left edge and can be understood by considering that complex eigenvalues of mode-coupling matrix H lead to evanescent evolutions in general, leaving only amplified supermodes on waveguides of largest gain [45]. Similar light transfer behaviors have been discussed in [45], but it is worth noting that mode excitations in our work are confined in a much smaller number of waveguides, yielding thus much tighter light transfer behaviors facilitating potential applications, applications, as spin- l matrices S_x and S_z are used to construct mode-coupling matrix H .

Light transfer behaviors in the \mathcal{PT} -symmetric wave-

guide array will become quite different, provided that each N th-order EP is split into a series of lower-order EPs as shown in Fig. 2(c) and Fig. 2(d). This is examined in Fig. 3(d) for an unbroken phase between 2nd-order EPs A_l^\pm and A_r^\pm ; in Fig. 3(e) at 2nd-order EPs E_l^\pm separating two partially broken phases; in Fig. 3(f) for a fully broken phase at the right of 2nd-order EPs G_r^\pm . We can see that evolutions of mode excitations vary from an asymmetric (breathing-like) bidirectional oscillation behavior, through an imperfect left-towards localization behavior, to a perfect left-towards localization behavior when Δ/Γ is increased to across one by one the 2nd and 3rd-order EPs. This nontrivial transition of light transfer behaviors depends critically on the order (degree of degeneracy) and the number of EPs. It is worth noting that the center-towards localization behaviors observed in Fig. 3(b) cannot be observed again in the absence of highest N th-order EPs.

Each N th-order EP in Fig. 2(a) and Fig. 2(b) for the \mathcal{PT} -symmetric waveguide array indicates also a sensitive transition with respect to distinct light transfer behaviors. This is justified in Fig. 4 by examining $|a_0(z)|^2 / \sum_n |a_n(z)|^2$ for a few typical ratios of Δ/Γ and another single-site initial excitation $a_n = \delta_{n,7}$. It is easy to see that the central waveguide exhibits a robust mode excitation with neither periodic oscillations nor a fast decay for $\Delta/\Gamma = 2$ referring to one N th-order EP Υ_r . Adjusting Δ/Γ to enter the unbroken or broken phase beyond this N th-order EP, we find instead periodic oscillations or a fast decay of mode excitation in the central waveguide. Hence it is viable to attain a robust output of mode excitation from the central waveguide or realize a sensitive switching between distinct light transfer behaviors in the \mathcal{PT} -symmetric waveguide array by accurately modulating Δ or Γ .

III. ANTI- \mathcal{PT} -SYMMETRIC WAVEGUIDE ARRAY

In this section, we try to construct an anti- \mathcal{PT} -symmetric mode-coupling matrix so as to further investigate highest N th-order EPs and nontrivial light transfer behaviors in an alternative array consisting of $N = 2l + 1$ single-mode waveguides. This can be done by rotating both S_x and S_z in the \mathcal{PT} -symmetric mode-coupling matrix H around S_y , yielding thus $S_x \rightarrow S_z$ and $S_z \rightarrow -S_x$. The resultant anti- \mathcal{PT} -symmetric mode-coupling matrix is

$$\tilde{H} = \Delta S_z - 2i\Gamma S_x = \begin{pmatrix} l\Delta & -i\Gamma_{1-l} & 0 & \cdots & 0 & 0 & 0 \\ -i\Gamma_{1-l} & (l-1)\Delta & -i\Gamma_{2-l} & \cdots & 0 & 0 & 0 \\ 0 & -i\Gamma_{2-l} & (l-2)\Delta & \ddots & \ddots & 0 & 0 \\ \vdots & \vdots & \ddots & \ddots & \ddots & \vdots & \vdots \\ 0 & 0 & \ddots & \ddots & -(l-2)\Delta & -i\Gamma_{l-2} & 0 \\ 0 & 0 & 0 & \cdots & -i\Gamma_{l-2} & -(l-1)\Delta & -i\Gamma_{l-1} \\ 0 & 0 & 0 & \cdots & 0 & -i\Gamma_{l-1} & -l\Delta \end{pmatrix}, \quad (4)$$

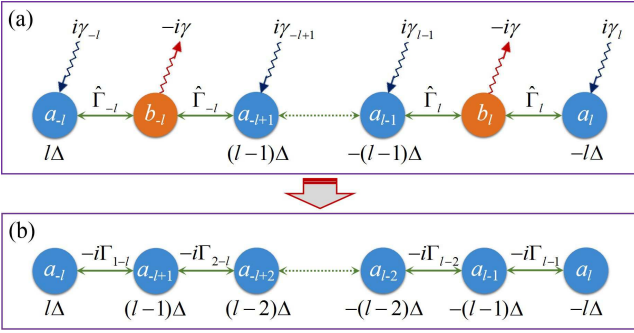


FIG. 5: (a) A non-Hermitian waveguide array consisting of $2l + 1$ primary modes a_n and $2l$ assistant modes b_n . Each b_n exhibits an imaginary propagation constant $-i\gamma$ (loss for $\gamma > 0$) and a real coupling constant $\hat{\Gamma}_n$ with two adjacent a_n , which exhibits instead a complex propagation constant $-n\Delta + i\gamma_n$ (gain for $\gamma_n > 0$). (b) An equivalent anti- \mathcal{PT} -symmetric waveguide array with imaginary coupling constants $-i\Gamma_n$ after eliminating the $2l$ assistant modes with properly designed γ_n and $\hat{\Gamma}_n$.

which reserves the underlying $SU(2)$ symmetry on one hand and satisfies the anti-commutation relation $\{\mathcal{PT}, \tilde{H}\} = 0$ on the other hand. Obviously, the $2l + 1$ diagonal elements $\tilde{H}_{n,n}$ become real so that all waveguide modes a_n suffer neither loss nor gain, while the $4l$ sub-diagonal elements $\tilde{H}_{n,n\pm 1}$ become imaginary so that waveguide modes a_n and $a_{n\pm 1}$ are passively coupled. However, passive couplings are usually not realistic, hence one question arises: is it viable to realize mode-coupling matrix \tilde{H} by modifying the waveguide array as shown in Fig. 1?

The answer is positive provided we insert an assistant waveguide described by mode b_n between each pair of pri-

mary waveguides described by modes a_n and a_{n-1} (a_{n+1}) for $n > 0$ ($n < 0$) as shown in Fig. 5(a) [65]. With respect to this $\hat{N} = 4l + 1$ waveguide array, we can write down the Schrödinger-like equation $i\partial_z \hat{\psi} = \hat{H} \hat{\psi}$ for a $\hat{N} \times \hat{N}$ mode-coupling matrix \hat{H} and a $\hat{N} \times 1$ column vector $\hat{\psi}$ and expand it into the following equations of motion

$$\frac{\partial a_n}{\partial z} = \begin{cases} (in\Delta + \gamma_n)a_n - i\hat{\Gamma}_{n-1}b_{n-1} - i\hat{\Gamma}_n b_n & (n < 0), \\ \gamma_n a_n - i\hat{\Gamma}_{n-1}b_{n-1} - i\hat{\Gamma}_{n+1}b_{n+1} & (n = 0), \\ (in\Delta + \gamma_n)a_n - i\hat{\Gamma}_n b_n - i\hat{\Gamma}_{n+1}b_{n+1} & (n > 0); \end{cases} \quad (5a)$$

$$\frac{\partial b_n}{\partial z} = \begin{cases} -\gamma b_n - i\hat{\Gamma}_n(a_n + a_{n+1}) & (n < 0), \\ -\gamma b_n - i\hat{\Gamma}_n(a_{n-1} + a_n) & (n > 0), \end{cases} \quad (5b)$$

where γ_n describes different gain constants of primary modes a_n while γ represents the common decay rates of assistant modes b_n . We have also introduced $\hat{\Gamma}_n$ to denote different coupling constants between modes b_n and a_n as well as b_n and a_{n+1} (a_{n-1}) for $n < 0$ ($n > 0$). In the limit of $\gamma \gg \hat{\Gamma}_n$, it is viable to attain with Eq. (5b)

$$b_n = \begin{cases} -i\hat{\Gamma}_n(a_n + a_{n+1})/\gamma & (n < 0), \\ -i\hat{\Gamma}_n(a_{n-1} + a_n)/\gamma & (n > 0), \end{cases} \quad (6)$$

by directly setting $\partial_z b_n = 0$ with the approximation of an adiabatic evolution [65, 68].

Substituting Eq. (6) back into Eq. (5a), we can further attain

$$\frac{\partial a_n}{\partial z} = \begin{cases} [in\Delta + \gamma_n - (\hat{\Gamma}_{n-1}^2 + \hat{\Gamma}_n^2)/\gamma]a_n - (\hat{\Gamma}_{n-1}^2/\gamma)a_{n-1} - (\hat{\Gamma}_n^2/\gamma)a_{n+1} & (n < 0), \\ [\gamma_n - (\hat{\Gamma}_{n-1}^2 + \hat{\Gamma}_{n+1}^2)/\gamma]a_n - (\hat{\Gamma}_{n-1}^2/\gamma)a_{n-1} - (\hat{\Gamma}_{n+1}^2/\gamma)a_{n+1} & (n = 0), \\ [in\Delta + \gamma_n - (\hat{\Gamma}_n^2 + \hat{\Gamma}_{n+1}^2)/\gamma]a_n - (\hat{\Gamma}_n^2/\gamma)a_{n-1} - (\hat{\Gamma}_{n+1}^2/\gamma)a_{n+1} & (n > 0), \end{cases} \quad (7)$$

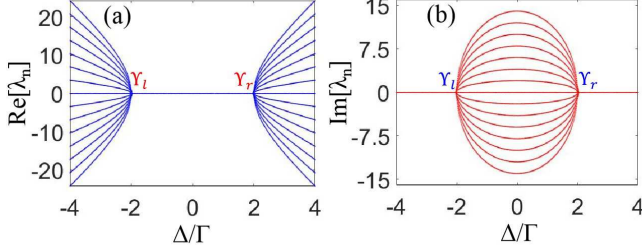


FIG. 6: (a) Real and (b) imaginary parts of $2l + 1$ eigenvalues of anti- \mathcal{PT} -symmetric mode-coupling matrix \tilde{H} in Eq. (4) against Δ/Γ with $\Gamma_n = \Gamma\sqrt{(l \pm n + 1)(l \mp n)}$ for $n \in \pm\{0, l - 1\}$ and $l = 7$.

by eliminating the $2l$ assistant modes b_n . Eq. (7) finally reduces into

$$\frac{\partial a_n}{\partial z} = \begin{cases} in\Delta a_n - \Gamma_n a_{n-1} - \Gamma_{n+1} a_{n+1} & (n < 0), \\ -\Gamma_n (a_{n-1} + a_{n+1}) & (n = 0), \\ in\Delta a_n - \Gamma_{n-1} a_{n-1} - \Gamma_n a_{n+1} & (n > 0), \end{cases} \quad (8)$$

when we take (i) $\gamma_n = (\hat{\Gamma}_{n-1}^2 + \hat{\Gamma}_n^2)/\gamma$ for $n < 0$, $\gamma_0 = (\hat{\Gamma}_{-1}^2 + \hat{\Gamma}_1^2)/\gamma$ for $n = 0$, and $\gamma_n = (\hat{\Gamma}_n^2 + \hat{\Gamma}_{n+1}^2)/\gamma$ for $n > 0$; (ii) $\hat{\Gamma}_n^2/\gamma = \Gamma_{n+1}$ for $n < 0$ and $\hat{\Gamma}_n^2/\gamma = \Gamma_{n-1}$ for $n > 0$. That means, we have $\hat{\Gamma}_{-n}^2 = \hat{\Gamma}_n^2$ and $\gamma_{-n} = \gamma_n$ for $n \in \pm\{1, l\}$ restricted again by $\Gamma_n = \Gamma\sqrt{(l \pm n + 1)(l \mp n)}$ for $n \in \pm\{0, l - 1\}$ as the array of \hat{N} coupled waveguides in Fig. 5(a) reduces to the array of N waveguides in Fig. 5(b). Eq. (8) is what we can attain by inserting the $N \times 1$ column vector $\psi = (a_{-l}, \dots, a_0, \dots, a_l)^T$ and the $N \times N$ mode-coupling matrix \tilde{H} into the Schrödinger-like equation $i\partial_z \psi = \tilde{H}\psi$, justifying the feasibility for realizing effectively neutral waveguide arrays with passive couplings.

We plot in Fig. 6(a) and Fig. 6(b), respectively, real and imaginary parts of eigenvalues λ_n of the anti- \mathcal{PT} -symmetric matrix \tilde{H} in Eq. (4) with $l = 7$. In comparison to that observed in Fig. 2(a) and Fig. 2(b), the common feature is that all fifteen eigenvalues coalesce again at $\Delta/\Gamma = \pm 2$ with $\lambda_n \equiv 0$ to yield two highest 15th-order EPs Υ_l and Υ_r ; the difference lies in that the unbroken and broken phases refer instead to purely imaginary and purely real eigenvalues, respectively [68]. To be more specific, the unbroken (broken) phase is attained with a smaller (larger) absolute ratio of imaginary propagation constant $-in\Delta$ and real coupling constant Γ_n

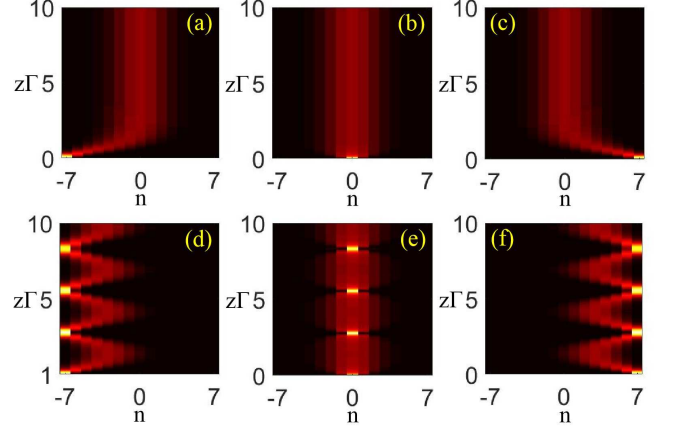


FIG. 7: Evolutions of mode excitations in an anti- \mathcal{PT} -symmetric waveguide array with $\Gamma_n = \Gamma\sqrt{(l \pm n + 1)(l \mp n)}$ for $n \in \pm\{0, l - 1\}$ and $l = 7$ regarding different initial excitations $a_n(0) = \delta_{n,-7}$ (a,d); $a_n(0) = \delta_{n,0}$ (b,e); $a_n(0) = \delta_{n,7}$ (c,f). The upper and lower panels are plotted with $\Delta/\Gamma = 1$ (a,b,c) and $\Delta/\Gamma = 3$ (d,e,f), respectively.

for H in Eq. (1), while with a smaller (larger) absolute ratio of real propagation constant $-n\Delta$ and imaginary coupling constant $-i\Gamma_n$ for \tilde{H} in Eq. (4). Therefore, distinct light transfer behaviors are expected to occur in the \mathcal{PT} -symmetric and anti- \mathcal{PT} -symmetric waveguide arrays even if they are engineered to work with the same parameters as discussed below.

We then examine with Eq. (8) evolutions of mode excitations characterized by $|a_n(z)|^2 / \sum_n |a_n(z)|^2$ in the anti- \mathcal{PT} -symmetric waveguide array for different single-site initial excitations $a_n(0) = \delta_{n,-7}$, $a_n(0) = \delta_{n,0}$, and $a_n(0) = \delta_{n,7}$ as shown in Fig. 7. In the unbroken phase with $\Delta/\Gamma = 1$, we can see from Figs. 7(a-c) that mode excitations always converge to and finally leave from a few middle waveguides without exhibiting oscillations and independent of initial single-site excitations. Such a robust center-towards localization behavior is clearly different from the left-edge-towards localization behavior observed in the broken phase of an \mathcal{PT} -symmetric waveguide array as shown in Fig. 3(c). The underlying physics for this center-towards localization behavior should be that all adjacent waveguides are passively coupled with the gradually reduced imaginary coupling constants $-i\Gamma_n = -i\Gamma_{-n}$ from both edges to the center. In the broken phase with $\Delta/\Gamma = 3$, we can see from Figs. 7(d-f) that mode excitations oscillate with an identical fixed period determined by the ratio Δ/Γ but of

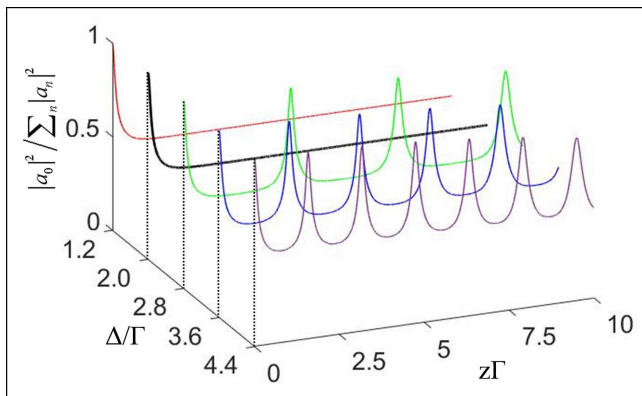


FIG. 8: Evolutions of central ($n = 0$) mode excitations referring to different ratios of Δ/Γ in an anti- \mathcal{PT} -symmetric waveguide array with $\Gamma_n = \Gamma\sqrt{(l \pm n + 1)(l \mp n)}$ for $n \in \pm\{0, l - 1\}$ and $l = 7$ regarding the initial excitation $a_n(0) = \delta_{n,0}$.

different centers identical to origins of single-site excitations. This more localized origin-centered oscillation may be attributed to a larger ratio $\Delta/\Gamma = 3$ and is also very different from that observed in the unbroken phase of an \mathcal{PT} -symmetric waveguide array as shown in Fig. 3(a).

To gain a more intuitive insight into the transition between different light transfer behaviors, we focus on the central ($n = 0$) waveguide by examining $|a_0(z)|^2/\sum_n |a_n(z)|^2$ in Fig. 8 for different values of Δ/Γ while a fixed initial excitation $a_n = \delta_{n,0}$. As the anti- \mathcal{PT} -symmetric waveguide array works at and below its N th-order EP Υ_r , consistent with that observed in Fig. 7(b) but different from that observed in Fig. 4, the central mode excitation quickly decays to a steady value ~ 0.5 independent of the ratio Δ/Γ . As the anti- \mathcal{PT} -symmetric waveguide array works above the N th-order EP Υ_r , consistent with that observed in Fig. 7(e) but different from that observed in Fig. 4, the central mode excitation starts to oscillate with a period $\delta z = 2\pi/\sqrt{\Delta^2 - 4\Gamma^2}$ tunable in an arbitrarily large range (unattainable yet in the \mathcal{PT} -symmetric waveguide array) since $\Delta/2\Gamma$ may approach

either unit or infinity. Hence, it is viable to attain a controlled output of mode excitation from the central waveguide by adjusting the ratio Δ/Γ , which may serve as an efficient scheme of high-precision measurement on relevant parameters determining Δ or Γ .

IV. CONCLUSIONS

In summary, we have studied nontrivial light transfer dynamics by working at and beyond one of two N th-order EPs, referring to highest-degree degeneracies of all N eigenvalues of relevant mode-coupling matrices, in two non-Hermitian waveguide arrays exhibiting a \mathcal{PT} or an anti- \mathcal{PT} symmetry. For the \mathcal{PT} -symmetric waveguide array with balanced gain and loss, light transfer dynamics is viable to switch between a unidirectional oscillation behavior in the unbroken phases, through a center-towards localization behavior at one N th-order EP, to an edge-towards localization behavior in the broken \mathcal{PT} phases. For the anti- \mathcal{PT} -symmetric waveguide array with passive couplings, light transfer dynamics is very different again in the broken and unbroken phases, hence supporting the transition between an origin-centered oscillation behavior and a center-towards localization behavior across one N th-order EP. These drastic transitions of light transfer behaviors are expected to facilitate advanced photonic applications like sensitive optical switching and high-precision measurement, while providing also new perspectives for further theoretical studies.

Acknowledgments

This work is supported by National Natural Science Foundation of China (NO. 11704064 and No. 12074061), Fundamental Research Funds for the Central Universities (NO. 2412019FZ045), and Science Foundation of the Education Department of Jilin Province (NO. JJKH20211279KJ).

-
- [1] C. M. Bender, “Making sense of non-Hermitian Hamiltonians,” *Rep. Prog. Phys.* **70**, 947-1018 (2007).
- [2] N. Moiseyev, *Non-Hermitian Quantum Mechanics* (Cambridge University Press, 2011).
- [3] L. Feng, R. El-Ganainy, and L. Ge, “Non-Hermitian photonics based on parity-time symmetry,” *Nat. Photonics* **11**, 752-762 (2017).
- [4] M. A. Quiroz-Juárez, A. Perez-Leija, K. Tschernig, B. M. Rodríguez-Lara, O. S. Magaña-Loaiza, K. Busch, Y. N. Joglekar, and R. de J. León-Montiel, “Exceptional points of any order in a single, lossy waveguide beam splitter by photon-number-resolved detection,” *Photon. Res.* **7**, 862-867 (2019).
- [5] Y. Ashida, Z. Gong, and M. Ueda, “Non-Hermitian physics,” *Adv. Phys.* **69**, 249-435 (2020).
- [6] L. Jin, X. Z. Zhang, G. Zhang, and Z. Song, “Reciprocal and unidirectional scattering of parity-time symmetric structures,” *Sci Rep.* **6**, 20976 (2016).
- [7] R. El-Ganainy, K. G. Makris, M. Khajavikhan, Z. H. Musslimani, S. Rotter, and D. N. Christodoulides, “Non-Hermitian physics and \mathcal{PT} symmetry,” *Nat. Phys.* **14**, 11-19 (2018).
- [8] I. I. Arkhipov, A. Miranowicz, O. Di Stefano, R. Stassi, S. Savasta, F. Nori, and Ş. K. Özdemir, “Scully-Lamb quantum laser model for parity-time-symmetric whispering-gallery microcavities: Gain saturation effects and nonreciprocity,” *Phys. Rev. A* **99**, 053806 (2019).
- [9] H. Zhou, J. Y. Lee, S. Liu, and B. Zhen, “Exceptional

- surfaces in \mathcal{PT} -symmetric non-Hermitian photonic systems,” *Optica* **6**, 190-193 (2019).
- [10] S. Soleymani, Q. Zhong, M. Mokim, S. Rotter, R. El-Ganainy, and Ş. K. Özdemir, “Chiral and degenerate perfect absorption on exceptional surfaces,” *Nat. Commun.* **13**, 599 (2022).
- [11] S. Longhi, “Quantum interference and exceptional points,” *Opt. Lett.* **43**, 5371-5374 (2018).
- [12] M.-A. Miri, and A. Alù, “Exceptional points in optics and photonics,” *Science* **363**, eaar7709 (2019).
- [13] Ş. K. Özdemir, S. Rotter, F. Nori, and L. Yang, “Parity-time symmetry and exceptional points in photonics,” *Nat. Mater.* **18**, 783-798 (2019).
- [14] C. M. Bender, and S. Boettcher, “Real Spectra in non-Hermitian Hamiltonians having \mathcal{PT} symmetry,” *Phys. Rev. Lett.* **80**, 5243-5246 (1998).
- [15] A. Mostafazadeh, “Pseudo-Hermiticity versus \mathcal{PT} symmetry: The necessary condition for the reality of the spectrum of a non-Hermitian Hamiltonian,” *J Math. Phys.* **43**, 205-214 (2001); “Pseudo-Hermiticity versus \mathcal{PT} -symmetry. II. A complete characterization of non-Hermitian Hamiltonians with a real spectrum,” *J Math. Phys.* **43**, 2814-2816 (2002); “Pseudo-Hermiticity versus \mathcal{PT} -symmetry III: Equivalence of pseudo-Hermiticity and the presence of antilinear symmetries,” *J Math. Phys.* **43**, 3944-3951 (2002).
- [16] L. Jin, “Asymmetric lasing at spectral singularities,” *Phys. Rev. A* **97**, 033840 (2018).
- [17] C. A. Downing, D. Zueco, and L. Martín-Moreno, “Chiral current circulation and symmetry in a trimer of oscillators,” *ACS Photonics* **7**, 3401-341 (2020).
- [18] F. Wang, X. Niu, X. Hu, T. Gu, X. Wang, J. Yang, H. Yang, Y. Ao, S. Wang, and Q. Gong, “All-optical mode-selective router based on broken anti- \mathcal{PT} symmetry,” *Phys. Rev. Appl.* **14**, 044050 (2020).
- [19] H. C. Wu, L. Jin, and Z. Song, “Topology of an anti-parity-time symmetric non-Hermitian Su-Schrieffer-Heeger model,” *Phys. Rev. B* **103**, 235110 (2021).
- [20] A. Bergman, Ro. Duggan, K. Sharma, M. Tur, A. Zadok and A. Alù, “Observation of anti-parity-time-symmetry, phase transitions and exceptional points in an optical fibre,” *Nat. Commun.* **12**, 486 (2021).
- [21] L. Feng, X. Zhu, S. Yang, H. Zhu, P. Zhang, X. Yin, Y. Wang, and X. Zhang, “Demonstration of a large-scale optical exceptional point structure,” *Opt. Express* **22**, 1760-1767 (2014).
- [22] K. Ding, G. Ma, M. Xiao, Z. Q. Zhang, and C. T. Chan, “Emergence, coalescence, and topological properties of multiple exceptional points and their experimental realization,” *Phys. Rev. X* **6**, 021007 (2016).
- [23] S. Lin, L. Jin, and Z. Song, “Symmetry protected topological phases characterized by isolated exceptional points,” *Phys. Rev. B* **99**, 165148 (2019).
- [24] M. Parto, Y. G. N. Liu, B. Bahari, M. Khajavikhan, and D. N. Christodoulides, “Non-Hermitian and topological photonics: optics at an exceptional point,” *Nanophotonics* **10**, 403-423 (2021).
- [25] R. Fleury, D. Sounas, and A. Alu, “An invisible acoustic sensor based on parity-time symmetry,” *Nat. Commun.* **6**, 5905 (2015).
- [26] K. Ding, G. C. Ma, Z. Q. Zhang, and C. T. Chan, “Experimental demonstration of an anisotropic exceptional point,” *Phys. Rev. Lett.* **121**, 085702 (2018).
- [27] C. Chen, L. Jin, and R.-B. Liu, “Sensitivity of parameter estimation near the exceptional point of a non-Hermitian system,” *New. J Phys.* **21**, 083002 (2019).
- [28] L. Chang, X. S. Jiang, S. Y. Hua, C. Yang, J. M. Wen, L. Jiang, G. Y. Li, G. Z. Wang, and M. Xiao, “Parity-time symmetry and variable optical isolation in active-passive-coupled microresonators,” *Nat. Photonics* **8**, 524-529 (2014).
- [29] L. Jin, P. Wang, and Z. Song, “One-way light transport controlled by synthetic magnetic fluxes and \mathcal{PT} -symmetric resonators,” *New. J Phys.* **19**, 015010 (2017).
- [30] H.-K. Lau, and A. A. Clerk, “Fundamental limits and non-reciprocal approaches in non-Hermitian quantum sensing,” *Nat. Commun.* **9**, 4320 (2018).
- [31] W. E. Hayenga, M. Parto, J. Ren, F. O. Wu, M. P. Hokmabadi, C. Wolff, R. El-Ganainy, N. A. Mortensen, D. N. Christodoulides, and M. Khajavikhan, “Direct Generation of Tunable Orbital Angular Momentum Beams in Microring Lasers with Broadband Exceptional Points,” *ACS Photonics* **6**, 1895-1901 (2019).
- [32] H. Hodaie, A. U. Hassan, S. Wittek, H. Garcia-Gracia, R. El-Ganainy, D. N. Christodoulides, and M. Khajavikhan, “Enhanced sensitivity at higher-order exceptional points,” *Nature* **548**, 187-191 (2017).
- [33] H. Jing, Ş. K. Özdemir, H. Lü, and F. Nori, “High-order exceptional points in optomechanics,” *Sci Rep.* **7**, 3386 (2017).
- [34] C. Zeng, Y. Sun, G. Li, Y. Li, H. Jiang, Y. Yang, and H. Chen, “Enhanced sensitivity at high-order exceptional points in a passive wireless sensing system,” *Opt. Express* **27**, 27562-27572 (2019).
- [35] I. I. Arkhipov, F. Minganti, A. Miranowicz, and F. Nori, “Generating high-order quantum exceptional points in synthetic dimensions,” *Phys. Rev. A* **104**, 012205 (2021).
- [36] M. H. Teimourpour, Q. Zhong, M. Khajavikhan, R. El-Ganainy, “Higher Order Exceptional Points in Discrete Photonics Platforms,” in: *Parity-time Symmetry and Its Applications*, D. Christodoulides, J. Yang, eds. (Springer Singapore, 2018) p. 261-275.
- [37] M. H. Teimourpour, Ş. K. Özdemir, and R. El-Ganainy, “Reverse \mathcal{PT} phase transition across exceptional points of any order,” *EPL (Europhysics Letters)* **119**, 34003 (2017).
- [38] G.-Q. Zhang, and J. Q. You, “Higher-order exceptional point in a cavity magnonics system,” *Phys. Rev. B* **99**, 054404 (2019).
- [39] X. Fang, N. J. R. K. Gerard, Z. Zhou, H. Ding, N. Wang, B. Jia, Y. Deng, X. Wang, Y. Jing, and Y. Li, “Observation of higher-order exceptional points in a non-local acoustic metagrating,” *Commun. Phys.* **4**, 271 (2021).
- [40] Y. Wu, P. Zhou, T. Li, We. Wan, and Y. Zou, “High-order exceptional point based optical sensor,” *Opt. Express* **29**, 6080-6091 (2021).
- [41] A. Roy, S. Jahani, Q. Guo, A. Dutt, S. Fan, M.-A. Miri, and A. Marandi, “Nondissipative non-Hermitian dynamics and exceptional points in coupled optical parametric oscillators,” *Optica* **8**, 415-421 (2021).
- [42] B. M. Rodríguez-Lara and J. Guerrero, “Optical finite representation of the Lorentz group,” *Opt. Lett.* **40**, 5682-5685 (2015).
- [43] E. M. Graefe, U. Günther, H. J. Korsch, and A. E. Niederle, “A non-Hermitian \mathcal{PT} symmetric Bose-Hubbard model: eigenvalue rings from unfolding higher-

- order exceptional points,” *J. Phys. A : Math. Theor.* **41**, 255206 (2008).
- [44] W. H. Steeb, and Y. Hardy, “Exceptional points, non-normal matrices, hierarchy of spin matrices and an eigenvalue problem,” *Int. J. Mod. Phys. C* **25**, 1450059 (2014).
- [45] A. Guo, G. J. Salamo, D. Duchesne, R. Morandotti, M. Volatier-Ravat, V. Aimez, G. A. Siviloglou, and D. N. Christodoulides, “Observation of \mathcal{PT} -symmetry breaking in complex optical potentials,” *Phys. Rev. Lett.* **103**, 093902 (2009).
- [46] C. E. Rüter, K. G. Makris, R. El-Ganainy, D. N. Christodoulides, M. Segev, and D. Kip, “Observation of parity–time symmetry in optics,” *Nat. Phys.* **6**, 192-195 (2010).
- [47] N. Asger Mortensen, P. A. D. Gonçalves, Mercedesh Khajavikhan, Demetrios N. Christodoulides, Christos Tserkezis, and Christian Wolff, “Fluctuations and noise-limited sensing near the exceptional point of parity-time-symmetric resonator systems,” *Optica* **5**, 1342-1346 (2018).
- [48] R. El-Ganainy, M. Khajavikhan, D. N. Christodoulides, and S. K. Ozdemir, “The dawn of non-Hermitian optics,” *Commun. Phys.* **2**, 37 (2019).
- [49] S. K. Gupta, Y. Zou, X.-Y. Zhu, M.-H. Lu, L.-J. Zhang, X.-P. Liu, and Y.-F. Chen, “Parity-time symmetry in non-Hermitian complex optical media,” *Adv. Mater.* **32**, 1903639 (2020).
- [50] A. Krasnok, N. Nefedkin, and A. Alù, “Parity-time symmetry and exceptional points [Electromagnetic perspectives],” *IEEE Antennas Propag. Mag.* **63**, 110-121 (2021).
- [51] L. Jin, and Z. Song, “Parity-time symmetry under magnetic flux,” *Phys. Rev. A* **93**, 062110 (2016).
- [52] M. A. K. Othman, and F. Capolino, “Theory of exceptional points of degeneracy in uniform coupled waveguides and balance of gain and loss,” *IEEE Trans. Antennas Propag.* **65**, 5289-5302 (2017).
- [53] E. J. Pap, D. Boer, and H. Waalkens, “Non-Abelian nature of systems with multiple exceptional points,” *Phys. Rev. A* **98**, 023818 (2018).
- [54] L. Jin, “Parity-time-symmetric coupled asymmetric dimers,” *Phys. Rev. A* **97**, 012121 (2018).
- [55] Z. Lin, A. Pick, M. Lončar, and A. W. Rodriguez, “Enhanced spontaneous emission at third-order dirac exceptional points in inverse-designed photonic crystals,” *Phys. Rev. Lett.* **117**, 107402 (2016).
- [56] R.-B. Wu, Y. Zheng, Q.-M. Chen, and Y.-x. Liu, “Synthesizing exceptional points with three resonators,” *Phys. Rev. A* **98**, 033817 (2018).
- [57] Q. Zhong, D.N. Christodoulides, M. Khajavikhan, K.G. Makris, R. El-Ganainy, “Power-law scaling of extreme dynamics near higher-order exceptional points,” *Phys. Rev. A*, **97** 020105 (2018).
- [58] S. M. Zhang, X. Z. Zhang, L. Jin, and Z. Song, “High-order exceptional points in supersymmetric arrays,” *Phys. Rev. A* **101**, 033820 (2020).
- [59] S. Chakraborty, and A. K. Sarma, “Delayed sudden death of entanglement at exceptional points,” *Phys. Rev. A* **100**, 063846 (2019).
- [60] Q. Li, C.-J. Zhang, Z.-D. Cheng, W.-Z. Liu, J.-F. Wang, F.-F. Yan, Z.-H. Lin, Y. Xiao, K. Sun, Y.-T. Wang, J.-S. Tang, J.-S. Xu, C.-F. Li, and G.-C. Guo, “Experimental simulation of anti-parity-time symmetric Lorentz dynamics,” *Optica* **6**, 67-71 (2019).
- [61] Y. Duan, X. Zhang, Y. Ding, and X. Ni, “Single-cavity bi-color laser enabled by optical anti-parity-time symmetry,” *Photon. Res.* **9**, 1280-1288 (2021).
- [62] H. S. Xu, and L. Jin, “Coupling-induced nonunitary and unitary scattering in anti- \mathcal{PT} -symmetric non-Hermitian systems,” *Phys. Rev. A* **104**, 012218 (2021).
- [63] Y. Wei, H. Zhou, Y. Chen, Y. Ding, J. Dong, and X. Zhang, “Anti-parity-time symmetry enabled on-chip chiral polarizer,” *Photon. Res.* **10**, 76-83 (2022).
- [64] S. Ke, D. Zhao, J. Liu, Q. Liu, Q. Liao, B. Wang, and P. Lu, “Topological bound modes in anti- \mathcal{PT} -symmetric optical waveguide arrays,” *Opt. Express* **27**, 13858-13870 (2019).
- [65] H. Fan, J. Chen, Z. Zhao, J. Wen, and Y.-P. Huang, “Anti parity-time symmetry in passive nanophotonics,” *ACS Photonics* **7**, 3035-3041 (2020).
- [66] Y. Yang, Y.-P. Wang, J. W. Rao, Y. S. Gui, B. M. Yao, W. Lu, and C. M. Hu, “Unconventional singularity in anti-parity-time symmetric cavity magnonics,” *Phys. Rev. Lett.* **125**, 147202 (2020).
- [67] Y. Song, We. Liu, L. Zheng, Y. Zhang, B. Wang, and P. Lu, “Two-dimensional non-Hermitian Skin Effect in a Synthetic Photonic Lattice,” *Phys. Rev. Applied* **14**, 064076 (2020).
- [68] F. Yang, Y. C. Liu, and L. You, “Anti- \mathcal{PT} symmetry in dissipatively coupled optical systems,” *Phys. Rev. A* **96**, 053845 (2017).
- [69] Y. Qin, H. Chen, D. Luo, C. Pan, H. Hu, Y. Zhang, and D. Wei, “Quantum interference in anti-parity-time symmetric coupled waveguide system,” *Opt. Express* **29**, 29175-29185 (2021).
- [70] H.-H. Yu, S. Gwak, H. Kim, J.-W. Ryu, C.-M. Kim, and C.-H. Yi, “Salient role of the non-Hermitian coupling for optimizing conditions in multiple maximizations of inter-cavity light transfer,” *Opt. Express* **29**, 19998-20009 (2021).
- [71] L. Pan, S. Chen, and X. Cui, “High-order exceptional points in ultracold Bose gases,” *Phys. Rev. A* **99**, 011601 (2019).
- [72] T. Pertsch, P. Dannberg, W. Elflein, A. Bräuer, and F. Lederer, “Optical Bloch oscillations in temperature tuned waveguide arrays,” *Phys. Rev. Lett.* **83**, 4752-4755 (1999).
- [73] T. Sheng-Po, and Y. Che-Hua, “Guided waves propagating in plate with temperature gradients,” in *2011 IEEE International Ultrasonics Symposium*, (2011), p. 1802-1804.
- [74] U. Peschel, T. Pertsch, and F. Lederer, “Optical Bloch oscillations in waveguide arrays,” *Opt. Lett.* **23**, 1701-1703 (1998).
- [75] R. Khomeriki, “Multiple Landau-Zener tunnelling in two weakly coupled waveguide arrays,” *Eur. Phys. J D* **61**, 193-197 (2011).